HHS Public Access

Author manuscript

Otol Neurotol. Author manuscript; available in PMC 2019 June 01.

Published in final edited form as:

Otol Neurotol. 2018 June ; 39(5): 558–564. doi:10.1097/MAO.0000000000001787.

Oval window size and shape: A micro-CT anatomical study with considerations for stapes surgery

Matthew J. Zdilla, D.C.[1,2,3,*], **Janusz Skrzat, Ph.D.**[4], **Magdalena Kozerska, M.Sc.**[4], **Bartosz Leszczyński, Ph.D.**[5], **Jacek Tarasiuk, D.Sc., Ph.D., M.Sc.**[6], and **Sebastian Wroński, Ph.D., M.Sc.**[6]

[1]Department of Natural Sciences and Mathematics, West Liberty University, West Liberty, West Virginia, 26074, USA [2]Department of Graduate Health Sciences, West Liberty University, West Liberty, West Virginia, 26074, USA [3]Pathology, Anatomy, and Laboratory Medicine (PALM) Department, West Virginia University School of Medicine, Morgantown, West Virginia, 26506, USA [4]Department of Anatomy, Jagiellonian University, Medical College, ul. Kopernika 12, 31-034 Kraków, Poland [5]M. Smoluchowski Institute of Physics, Jagiellonian University, ul. Łojasiewicza 11, 30-348 Kraków, Poland [6]AGH University of Science and Technology, Faculty of Physics and Applied Computer Science, al. Mickiewicza 30, 30-065 Kraków, Poland

Abstract

Background—The oval window an important structure with regard to stapes surgeries, including stapedotomy for the treatment of otosclerosis. Recent study of perioperative imaging of the oval window has revealed that oval window niche height can indicate both operative difficulty and subjective discomfort during otosclerosis surgery. With regard to shape, structures incorporated into the oval window niche, such as cartilage grafts, must be compatible with the shape of the oval window. Despite the clinical importance of the oval window, there is little information regarding its size and shape.

Methods—This study assessed oval window size and shape via micro-CT paired with modern morphometric methodology in the fetal, infant, child, and adult populations. Additionally, the study compared oval window size and shape between sexes and between left- and right-sided ears.

Results—No significant differences were found among traditional morphometric parameters among age groups, sides, or sexes. However, geometric morphometric methods revealed shape differences between age groups. Further, geometric morphometric methods provided the average oval window shape and most-likely shape variance.

Conclusion—Beyond demonstrating oval window size and shape variation, the results of this report will aid in identifying patients among whom anatomical variation may contribute to surgical difficulty and surgeon discomfort, or otherwise warrant preoperative adaptations for the incorporation of materials into and around the oval window.

[*]Correspondence to: Matthew J. Zdilla, D.C., Associate Professor of Biology & Physician Assistant Studies, West Liberty University, Department of Natural Sciences and Mathematics, CSC 139; P.O. Box 295, West Liberty, WV (USA) 26074. Tel.: +1 304-336-8631; Fax: +1 304-336-8266; mzdilla@westliberty.edu.

The authors declare no conflicts of interest.

MeSH Keywords

ossicular prosthesis; otosclerosis; stapedotomy; stapes; stapes surgery

Introduction

The oval window (OW), otherwise known as the fenestra vestibuli or fenestra ovalis, is bounded superiorly by prominence of the tympanic segment of the facial canal, which lies just above the superior edge of the oval window, inferiorly by the promontory, anterosuperiorly by the cochleariform process, posteriorly by the ponticulus, pyramidal eminence and sinus tympani, and medially by the vestibule (1,2). The lumen of the OW is closed by the footplate of the stapes which is attached to its rim by the annular ligament, allowing movement (3).

The OW is subject to a variety of pathologies which may affect individuals of all ages. Such pathologies include atresia, congenital ankylosis of the stapes, and otosclerosis— conditions that are typically managed through surgical intervention (1,4–7).

Recent study of perioperative imaging of the OW has revealed that the OW niche height can predict operative difficulty in otosclerosis surgery (8). Likewise, OW niche height may serve as an indicator for the risk for technical difficulties during the stapes footplate approach (9).

In addition to the height of the OW, the anatomy of the inferior border of the OW is of particular surgical importance. With regard to stapedectomy, when a floating or depressed footplate is encountered, it has been recommended that a “pothole” be drilled in the inferior margin of the OW (10). The inferior border of the OW has also been utilized as a reference point for regional anatomical measurements (11). For example, the inferior border of the OW has been used as a landmark in which gapping distance with the stapes crura was compared between otosclerotic and non-otosclerotic ears and found to be statistically significant (12).

As the name suggests, the OW could be assumed to be “oval” in shape. However, it has also been described as “kidney-shaped” or “rectangular” (1,13). Aside from the subjective descriptions of “oval,” “kidney-shaped,” and ”rectangular,” there has been little objective, quantifiable study of the OW shape. Moreover, understanding the shape of the OW is clinically important. The OW may be obscured by variation in local neurovascular structures including a ptotic facial nerve or persistent stapedial artery, resulting in considerable difficulty for the surgeon attempting to fenestrate the stapes (14, 15). Therefore, an understanding of oval window shape variation can eschew intraoperative confusion. Additionally, the OW may be fit with, for example, a cartilage shoe for the stabilization of a total ossicular replacement prosthesis (16). In the case in which a structure is designed to fit within the OW, the native shape of the OW becomes inherently important.

Consideration of the size and shape of the OW is clinically important. However, there is little information regarding the size and shape of the OW, in general— much less among varied age groups. Therefore, this study assesses the size and shape variation of the OW in

the fetal/infant, child, and adult populations. Additionally, this study provides a comparison of OW size and shape both side-to-side and between sexes. The results of this study will aid in preoperative assessment and planning.

Materials and Methods

Oval windows from a total of 44 dry human temporal bones were included in the study. Of the 44 temporal bones, 11 (five unilateral left-sided and three bilateral) were from fetuses and infants (age range: 32 weeks gestation to 1 year; sex: unknown), 16 (four unilateral right-sided and six bilateral) were from children (age range: 1.5 to 9 years; sex: five female, nine male, and two unsexed), and 17 (one unilateral left-sided and eight bilateral) were from adults (sex: nine female, eight male). All bone samples were well preserved and without post-mortem deformation, noteworthy anatomical variation, or pathology.

The petrous parts were dissected from the temporal bones and scanned with two micro-CT scanners. Twenty-eight bones were scanned with a Skyscan 1172 (N.V., Aartselaar, Belgium) and 16 were scanned with a Nanotom 180N (GE Sensing & Inspection Technologies Phoenix X-ray Gmbh).

The Skyscan 1172 scanner was equipped with the X-ray detector: 11 Megapixel (4024 × 2680 in total; 4000 × 2400 effective), 12-bit digital X-ray camera with 24 × 36 mm field of view. The X-ray source voltage was set to 80 kV and current to 100 μA. The projection images were acquired over an angular range of 180° with an angular step of 0.5°. In the resultant images pixel size was 27 μm. From tomography projections captured along the long axis of the petrous bone cross-section images were reconstructed by Feldkamp algorithm using NRecon software delivered with the micro-CT scanner (17).

The Nanotom 180N provides unique spatial and contrast resolution of the scanned samples because of the installed ultra-high performance nanofocus X-ray tube (180 kV/57 W) and tungsten target with diamond window. The working parameters of X-ray tube were I=250 μA and V=70 kV. The reconstruction of scanned samples was done with the aid of proprietary GE software datosX ver. 2.1.0 using the Feldkamp algorithm for cone beam X-ray CT (17). The tomograms were registered on a Hamamatsu 2300×2300 pixel detector. The final resolution of the reconstructed objects was 18 μm.

Oval windows were visualized by volumetric reconstruction of the medial wall of the tympanic cavity from the micro-CT scans (Figure 1A) (18). Volumetric reconstruction was accomplished with CTvox software (Bruker Corporation, http://www.skyscan.be/products/downloads.htm). Planar images of the OW were obtained by using clipping planes crossing the reconstructed petrous bone. The position of the clipping planes were interactively changed in order to obtain *en face* projections of the OW. Therefore, the border of each OW was entirely visible as a closed loop (Figure 1B). Further, the contour of each OW was traced automatically on the volume rendered images.

For automatic tracing of the oval outline, the wand tool was implemented in ImageJ software (19). The wand tool creates a selection by tracing objects of uniform or similar brightness. In

result we obtained segmented image of the OW presented as a black line on white background, which was saved in separate graphical file as a binary image (Figure 1C).

The outlines of the OW were measured with ImageJ software (19). The size of the OW was assessed through the measurement of area, perimeter, width, and height. Width and height were determined by measuring the sides of a bounding box (Figure 1D). Shape descriptors including circularity (4π*area/perimeter^2), roundness (4*area/π*major axis^2), and aspect ratio (major axis/minor axis) were calculated by methods recently reported for the analysis of the shape of the foramen ovale of the sphenoid (20).

Normative descriptive statistics for all size and shape parameters were calculated. Likewise, paired t-tests were utilized to compare bilateral OW. Unpaired t-tests were used to compare differences among sexes. One-sided ANOVA was performed to assess differences between age groups. The aforementioned descriptive and inferential statistics were performed with GraphPad Prism statistical software, version 6.00 (GraphPad Software, La Jolla, CA, USA).

Geometric morphometric analysis was performed to further elucidate OW shape and shape variance. Oval window contours were traced through the use of TPSdig2 software (version 2.22)(21), beginning from the intersection between the margin of the OW and a line spanning the axis of a best fit ellipse according to the protocol utilized by Zdilla and Fijalkowski (22). The points along the curve were then resampled to include 300 equidistant points.

A consensus shape amidst a cloud of data points was generated from a Procrustes superimposition aligned by principal axes with the Geomorph package for R software (23). MorphoJ software was utilized for principle component analysis, canonical variate analysis, and discriminant function analysis (24). Canonical variate analysis and discriminant function analysis were utilized to compare differences in shape between age groups and left- and right-sided oval windows, respectively. Shape expansion/contraction along principle component axes was assessed with PAST3 Software (25).

Results

Descriptive statistics summarizing the average size and shape of left- and right-sided oval windows in each age group studied can be found in Table 1. Among the 17 paired left- and right-sided oval windows, paired t-tests revealed no significant differences between sides (Supplement 1). ANOVA revealed no differences among the fetal/infant, child, and adult groups with regard to any size parameters measured including area ($F(2, 41)=1.25$; $p=0.298$), width ($F(2,41)=0.51$; $p=0.6016$), and height ($F(2, 41)=1.91$; $p=0.1611$). Likewise, ANOVA revealed no differences among age grouping with regard to shape descriptors including circularity ($F(2, 41)=0.37$; $p=0.6911$), roundness ($F(2, 41)=0.18$; $p=0.8384$), and aspect ratio ($F(2, 41)=0.3024$; $p=0.7407$).

With regard to size and shape of the OW among sexes, normative descriptive statistics are summarized in Table 2. Concerning differences between sexes in size and shape, no statistically significant differences were noted in area, width, height, circularity, roundness, nor aspect ratio (Supplement 2).

Procrustes superimposition revealed the average shape of the OW as is seen in Figure 2A. Principle component analysis demonstrated that the greatest shape variance among oval windows was that of an approximation of the superior and inferior borders relative to the expansion of the anterior and postero-inferior borders of the OW and vice-versa (Figure 2B). Principle component 2 revealed a movement of a relatively sharp angulation of the OW border from the postero-superior aspect of the shape to the superior aspect of the shape. With regard to convexity/concavity, PC1 reveals a noteworthy difference among oval windows such that many are entirely convex, while some may have a concavity of the inferior border (Figure 2B). Parrot plots illustrating the relative expansion/contraction of the oval window shape in addition to the concavity/convexity of the inferior border of the OW, can be seen in Figure 3.

Discriminant function analysis revealed no significant difference between left- and right-sided means (Procrustes distance= 0.00971848; Mahalanobis distance= 2.5054; Hotelling's T-squared statistic= 68.9042; p= 0.9999). Canonical variate analysis revealed differences in oval window shapes among age groups (Figure 2C, Table 3). Children tended to have a more concave inferior border when compared to fetal/infant and adult groups (Figure 2C). Also, children tended to have a sharper infero-posterior angle relative to other age groups (Figure 2C).

Discussion

The OW, footplate of the stapes, and annular ligament create the complex system which is responsible for transmission of the acoustic energy from the middle ear to inner ear. The mechanical behavior of the footplate depends on its shape and orientation in the OW; therefore, its articulation at the OW has been the subject of the past and current studies (26,27). Moreover, the anatomy of the OW has been demonstrated to influence the surgical difficulty of stapes surgeries (8,9,28). A paucity of studies have assessed the anatomy of the OW. The present study is unique in its assessment of both the morphometry and morphology of the OW from individuals, both female and male, spanning ages across the lifespan.

A few studies have assessed the anatomy of the OW while taking into consideration the size of the OW with respect to technical difficulty and discomfort during surgery. Therefore, it is important to assess the size data from this study with respect to those studies that have correlated OW dimensions to surgical difficulty.

Ukkola-Pons et al (9) found that an OW height less than 1.4mm should be considered a risk factor for technical difficulties during stapes footplate approaches. This study assessed the height of the OW from a bounding box, but also noted that the inferior aspect of the OW may have a concavity, that is into the lumen of the OW niche. Therefore, some measurements from this study may err toward larger measurements than those studies measuring the height of the OW from, for example the middle-superior to the middle-inferior boundaries of the OW. Still, the average of the fetal/infant and child populations fell at or below 1.4mm (fetal/infant = 1.36 ± 0.18mm; child 1.40 ± 0.20mm, respectively). The average adult height was 1.50 ± 0.19, above the 1.4mm mark noted by Ukkola-Pons et al (9). The results of this study, in light of the Ukkola-Pons et al (9) criterion of <1.4mm OW

height as a risk factor for surgical difficulty, would suggest that 63.6% (7:11) of fetal/infant, 56.3% (9:16) of child, and 41.2%% (7:17) of adult oval windows would present with surgical difficulty (Supplement 3). Further, of the 44 oval windows studied, a total of 23 (52.3%) would present technical difficulty (Supplement 3).

Parra et al (8), used CT scan measurements of the OW width and noted that the cut-off threshold of OW "width" with regard to intraoperative subjective discomfort was computed as 1.1mm. The measurement of "width" from the study by Parra et al, roughly translates to the *en face* height measurement performed in this study, since Parra was referring to width as a measurement visible in coronal images (8). In light of the Parra et al (8) criterion of 1.1mm leading to surgical discomfort, 9.1% (1:11) of fetal/infant and 6.3% (1:16) of child OW may cause surgical discomfort, while no adult OW fell below the 1.1mm measurement (Supplement 3).

With regard to shape, studies have identified the OW as being "kidney-shaped" and "rectangular." The results of this study suggests that due to the concavity of the inferior border of the OW, the shape may resemble that of a kidney in that the hilum of the kidney is concave, while the rest is convex in shape. Likewise, the term "rectangular" has merit as well in that the oval window is longer in its width dimension than that of its height and much of its shape variance may create relatively acute angles at the antero-inferior, antero-superior, postero-inferior, and postero-superior as demonstrated by shape change along –PC1 and –PC2 (Figures 2B and 3). So, the oval window shape encompasses that of being oval-, kidney-, and rectangular-shaped.

The average shape and most likely shape variance demonstrated in this report should be taken into account when adapting materials to be placed in and around the OW. For example, the stapes footplate has been entirely reconstructed from cartilage— a procedure requiring precise fitting that is compatible with the OW (29). Rusiecka and Bernal-Sprekelsen (29) report utilizing a 1.5 × 3.5mm piece of cartilage for this purpose. Similarly, Beutner et al (16) developed a cartilage guide for the stabilization of a total ossicular replacement prosthesis in the OW niche. Their description noted that the cartilage guide was "oval-shaped" and measured 2.5 3.5mm (16). In light of the information from this report, a cartilage insert of an oval shape with such a relatively large size, may be ill-suited for a small, kidney-shaped (i.e. inferiorly concave) OW. The shape of the OW may also influence its role as a route for drug administration (30). Recently, trans-oval-window implants have been created for the purpose of drug administration (31). Therefore, the information from this study should be taken into consideration in the creation of such implants, with regard to both size and shape.

It is also important to keep in mind that the boundaries of the OW are created by clinically important structures nearby. Therefore, relative changes in the shape of the OW may be reflective of anatomical variation in the tympanic segment of the facial canal superiorly, the promontory inferiorly, cochleariform process antero-superiorly, the ponticulus, pyramidal eminence and sinus tympani posteriorly, the vestibule medially (1,2). The lumen of the oval window is closed by the footplate of the stapes which is attached to its rim by the annular

ligament (3). Therefore, shape change of the oval window is reflective of the variance in relative location of the aforementioned structures.

In summary, the anatomy of the OW, both in regard to its size and its shape may influence procedures including stapedotomy, stapedectomy, and placement of implants within and around the OW niche. By demonstrating oval window size and shape variation, the results of this report will aid in preoperative assessment and planning.

Supplementary Material

Refer to Web version on PubMed Central for supplementary material.

Acknowledgments

The research was carried out with the equipment purchased thanks to the financial support of the European Regional Development Fund in the framework of the Polish Innovation Economy Operational Program [contract no. POIG.02.01.00-12-023/08], the West Virginia IDeA Network for Biomedical Research Excellence [P20GM103434], and the NIH-NIAID [5K22AI087703]. The study was conducted with approval (KBET/198/B/2014) of the Bioethics Committee of the Jagiellonian University.

Citations

1. Zeifer B, Sabini P, Sonne J. Congenital absence of the oval window: radiologic diagnosis and associated anomalies. AJNR Am J Neuroradiol. 2000; 21:322–7. [PubMed: 10696017]
2. Mansour, S., Magnan, J., Haidar, H., Nicolas, K., Louryan, S. Comprehensive and clinical anatomy of the middle ear. Berlin: Springer; 2013.
3. Maroonroge, S., Emanuel, D., Rash, CE., Russo, MB., Letowski, T., Schmisser, E. Helmet-Mounted Displays: Sensation, Perception and Cognition Issues. Fort Rucker, Alabama: USAARL; 2009. p. 279-306.
4. Booth TN, Vezina LG, Karcher G, Dubovsky EC. Imaging and clinical evaluation of isolated atresia of the oval window. AJNR Am J Neuroradiol. 2000; 21:171–4. [PubMed: 10669245]
5. de Alarcon A, Jahrsdoerfer RA, Kesser BW. Congenital absence of the oval window: diagnosis, surgery, and audiometric outcomes. Otol Neurotol. 2008; 29:23–8. [PubMed: 18199954]
6. Thomeer H, Kunst H, Verbist B, Cremers C. Congenital oval or round window anomaly with or without abnormal facial nerve course: surgical results for 15 ears. Otol Neurotol. 2012; 33:779–84. [PubMed: 22664905]
7. Yang F, Liu Y, Sun J, Li J, Song R. Congenital malformation of the oval window: experience of radiologic diagnosis and surgical technique. Eur Arch Otorhinolaryngol. 2016; 273:593–600. [PubMed: 25763570]
8. Parra C, Trunet S, Granger B, et al. Imaging Criteria to Predict Surgical Difficulties During Stapes Surgery. Otol Neurotol. 2017; 38:815–21. [PubMed: 28414695]
9. Ukkola-Pons E, Ayache D, Pons Y, Ratajczak M, Nioche C, Williams M. Oval window niche height: quantitative evaluation with CT before stapes surgery for otosclerosis. AJNR Am J Neuroradiol. 2013; 34:1082–5. [PubMed: 23179652]
10. Saunders NC, Fagan PA. Promontory drilling in stapedectomy: an anatomical study. Otol Neurotol. 2006; 27:776–80. [PubMed: 16936565]
11. Chen Y, Chen S, Si Y, Liu Y, Xiong H, Zhang Z. Measurements of the position relationship between the inferior margin of the oval window and the endosteum of basal cochlear turn in histologic and HRCT study. Otol Neurotol. 2013; 34:1528–33. [PubMed: 24026027]
12. Anand V, Udayabhanu HN. Obliquity of the stapes in otosclerosis: intra-operative observations and implications in stapes surgery. J Laryngol Otol. 2016; 130:134–44. [PubMed: 26567711]
13. Standring, S., editor. Gray's Anatomy: The Anatomical Basis of Clinical Practice. 40th. New York: Churchill-Livingston/Elsevier; 2008. p. 624-5.

14. Horn KL. Management of the ptotic facial nerve and the persistent stapedial artery. Opper Tech Otolaryngol Head Neck Surg. 1998; 9:58–63.
15. Inagaki T, Kawano A, Ogawa Y, et al. Stapes fixation accompanied with abnormal facial nerve pathway. Auris Nasus Larynx. 2014; 41:313–6. [PubMed: 24581447]
16. Beutner D, Luers JC. Cartilage 'shoe': a new technique for stabilisation of titanium total ossicular replacement prosthesis at centre of stapes footplate. J Laryngol Otol. 2008; 122:682–6. [PubMed: 18485257]
17. Feldkamp LA, Davis LC, Kress JW. Practical cone-beam algorithm. J Opt Soc Am. 1984; A6:612–9.
18. Skrzat J, Kozerska M, Wroński S, Tarasiuk J, Walocha J. Volume rendering of the tympanic cavity from micro-CT data. Folia Med Cracov. 2015; 55:81–9. [PubMed: 26867122]
19. Rasband, WS. ImageJ. National Institutes of Health; Bethesda, Maryland, USA: 2004. Available at: http://rsb.info.nih.gov/ij/
20. Zdilla MJ, Hatfield SA, McLean KA, Cyrus LM, Laslo JM. A Morphometric Analysis with Neurosurgical Considerations. J Craniofac Surg. 2016; 27:222–8. [PubMed: 26703050]
21. Rohlf, FJ. TpsDig, Version 2.22. 2015. Available at http://life.bio.sunysb.edu/morph/
22. Zdilla MJ, Fijalkowski KM. The shape of the foramen ovale: a visualization aid for cannulation procedures. J Craniofac Surg. 2017; 28:548–51. [PubMed: 28027173]
23. Adams DC. Geomorph: an R package for the collection and analysis of geometric morphometric shape data. Methods Ecol Evol. 2013; 4:393–9.
24. Klingenberg CP. MorphoJ: an integrated software package for geometric morphometrics. Mol Ecol Resour. 2011; 11:353–7. [PubMed: 21429143]
25. Hammer Ø, Harper DAT, Ryan PD. PAST: Paleontological statistics software package for education and data analysis. Palaeontologia Electronica. 2001; 4:9.
26. Gyo K, Aritomo H, Goode RJ. Measurement of the ossicular vibration ratio in human temporal bones by use of a video measuring system. Acta Otolaryngol. 1987; 103:87–95. [PubMed: 3564932]
27. Gan RZ, Yang F, Zhang X, Nakmali D. Mechanical properties of stapedial annular ligament. Med Eng Phys. 2011; 33:330–9. [PubMed: 21112232]
28. Mancheño M, Aristegui M. Its Implication for the Vibroplasty Technique. Otol Neurotol. 2017; 38:e50–7. [PubMed: 28346291]
29. Rusiecka M, Bernal-Sprekelsen M. Footplate reconstruction: preliminary results. Otol Neurotol. 2014; 35:1797–800. [PubMed: 24979127]
30. Mohammadi A, Jufas N, Sale P, Lee K, Patel N, O'Leary S. Micro-CT analysis of the anatomical characteristics of the stapedial annular ligament. Anat Sci Int. 2017; 92:262–6. [PubMed: 26880086]
31. Sircoglou J, Gehrke M, Tardivel M, Siepmann F, Siepmann J. Extended Dexamethasone Release From Silicone-based Implants. Otol Neurotol. 2015; 36:1572–9. [PubMed: 26375981]

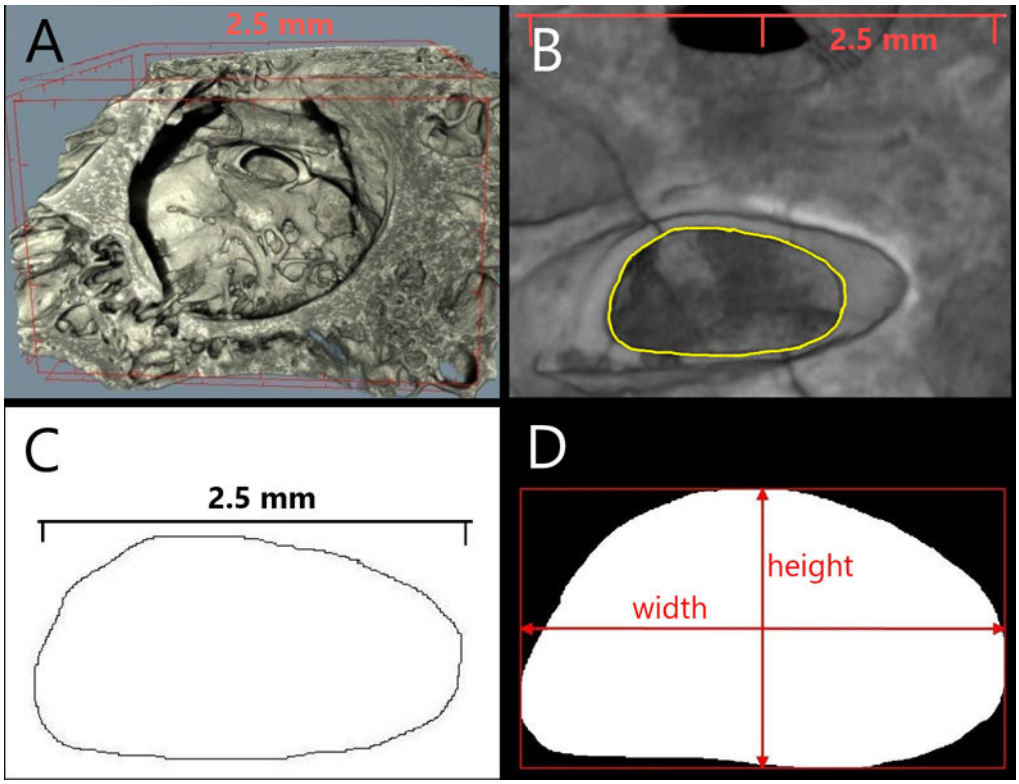

Figure 1.

Visualization of the oval window. **A**: Volume rendering of the exposed tympanic cavity including the oval window; **B**: *En face* planar view of the oval window with its margin outlined; outline of the oval window positioned frontally in the cutting plane; **C**: Binarized outline of the oval window margin; **D**: Schematic representation of the linear measurements of the oval window measured within the bounding box—the rectangular border that fully encloses a digital image of the oval window.

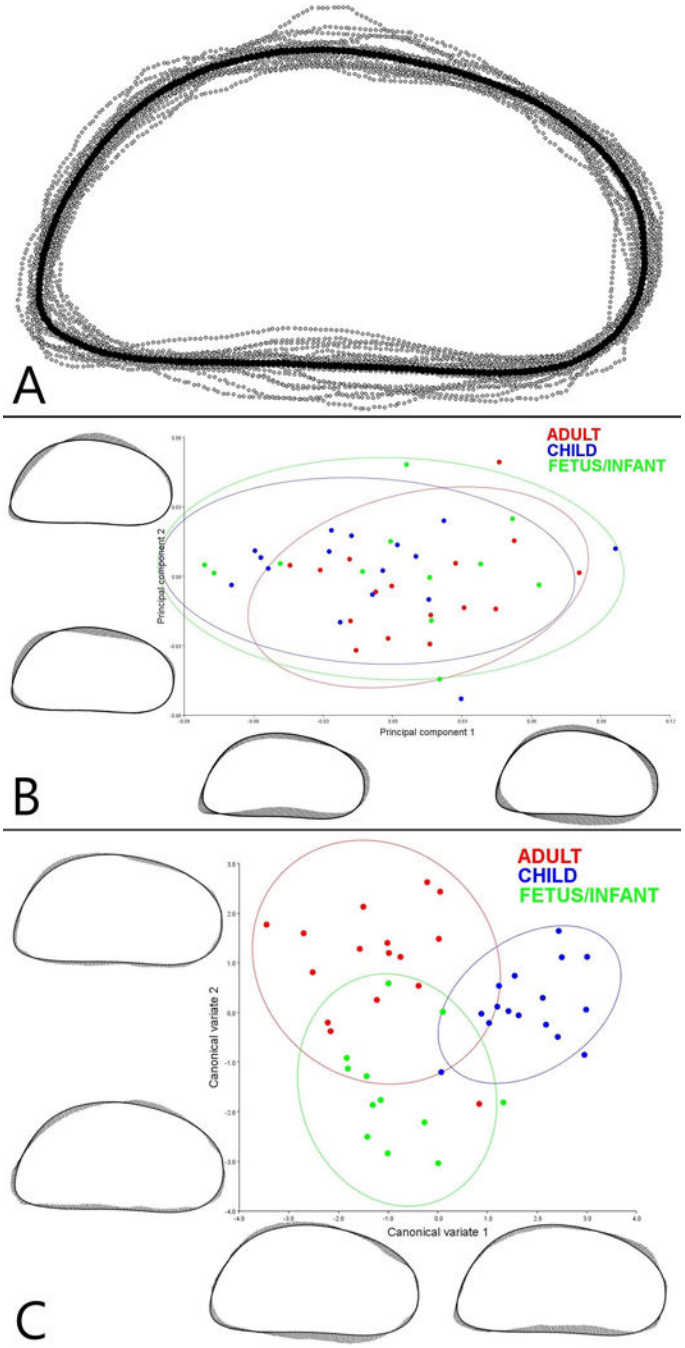

Figure 2.

Geometric morphometric analysis demonstrating average shape and shape variance among age groups. **A**: Consensus shape of the oval window (**black curve**) amidst a coordinate point cloud formed from 44 oval windows, each outlined with 300 coordinate points (**gray dots**). The left side of the image corresponds to the posterior, the right side of the image corresponds to the anterior, the top of the image corresponds to the superior, and the bottom of the image corresponds to the inferior; **B**: Results of a principle components analysis of 44 oval windows sorted into three age groups, each with a 90% confidence ellipse, respectively.

The first two principle components account for 79.1% of total shape variation. Principle component 1 accounts for 63.6% of shape variation and principle component 2 accounts for 15.5% of shape variation. Lollipop deformations identifying shape variance are displayed at the extremes of their respective axes. The greatest shape variation, as illustrated by the thin plate splines along PC1 occurs in an inverse fashion between the inferior and superior margins of the oval window as well as between the anterior and postero-inferior margins of the window. The extremes of principle component one demonstrate shape variance ranging from an entirely convex shape to a shape with an inferior concavity. Additionally, variance is noteworthy along the postero-inferior aspect of the oval window, ranging from an acute curvature to that of a more obtuse curvature. Principle component 2 demonstrates a change in a superior angle that shifts the angle from postero-superior to directly superior to the center of the shape; **C**: Results of a canonical variate analysis among 44 oval windows separated into three age groups (Fetus/Infant: n=12; Child: n=16; and Adult: n=16) with 90% confidence ellipses corresponding to each respective population. The first two canonical variates, illustrating the variation among groups (scaled by the inverse of the within-group variation), account for 100% of the total variance (CV1: 64.43%; CV2: 34.57%). Lollipop deformations along the canonical variate axes illustrate shape change between the age groups. To accentuate shape change, deformations were doubled and therefore illustrate +8 and −8 on CV1 and +6 and -8 on CV2, respectively. CV1 demonstrates a noteworthy change occurring in the concavity/convexity of the inferior margin of the oval window— the child group tending toward concavity, while the fetus/infant and adult groups tend toward inferior convexity.

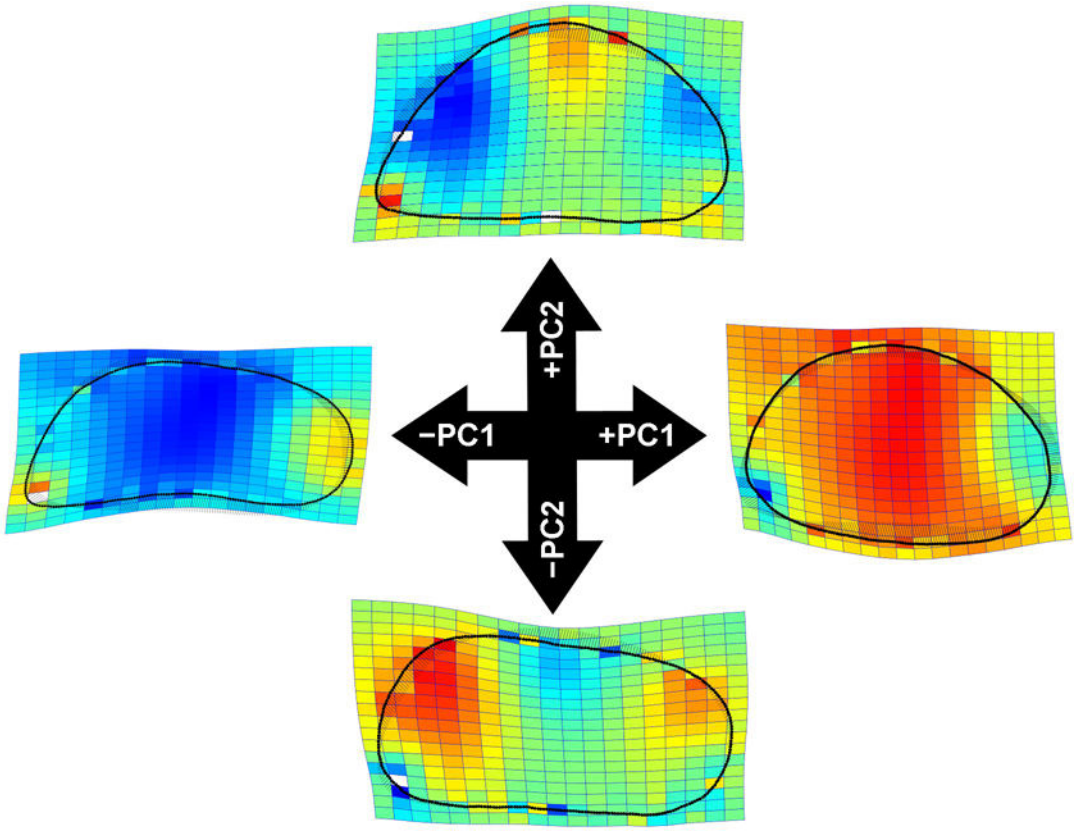

Figure 3.

Parrot plots of the oval windows located at the extremes of principle components 1 and 2 which explains 79.1% of total shape variation (PC1: 63.6%; PC2: 15.5%). The red hues represent magnitude of local expansion, blue hues represent local contraction, and greens represent invariant regions relative to the reference configuration (zero on the PC axis).

Table 1

Oval window size and shape descriptive statistics according to age grouping with respect to laterality.

Age Grouping	Side	n	Size Parameters (Mean±SD)			Shape Parameters (Mean±SD)		
			Area (mm^2)	Width (mm)	Height (mm)	Circularity	Roundness	Aspect Ratio
Fetal/Infant	L	8	2.90±0.31	2.62±0.19	1.41±0.14	0.76±0.05	0.54±0.06	1.88±0.20
	R	3	2.14±0.91	2.28±0.64	1.21±0.23	0.74±0.06	0.54±0.09	1.91±0.34
	L+R	11	2.69±0.60	2.53±0.36	1.36±0.18	0.75±0.05	0.54±0.06	1.89±0.23
Child	L	6	2.80±0.83	2.60±0.30	1.35±0.23	0.72±0.03	0.51±0.04	1.98±0.16
	R	10	2.91±0.50	2.62±0.13	1.44±0.18	0.76±0.04	0.55±0.06	1.85±0.20
	L+R	16	2.87±0.62	2.61±0.20	1.40±0.20	0.74±0.04	0.53±0.06	1.90±0.19
Adult	L	9	3.06±0.47	2.62±0.18	1.50±0.21	0.76±0.03	0.54±0.04	1.87±0.13
	R	8	3.04±0.69	2.62±0.30	1.49±0.19	0.75±0.03	0.55±0.05	1.83±0.15
	L+R	17	3.05±0.57	2.63±0.23	1.50±0.19	0.75±0.03	0.54±0.04	1.85±0.14
Total Population	L	23	2.93±0.53	2.62±0.21	1.43±0.20	0.75±0.04	0.53±0.05	1.90±0.17
	R	21	2.85±0.67	2.57±0.31	1.43±0.20	0.75±0.04	0.55±0.06	1.85±0.20
	L+R	44	2.89±0.60	2.60±0.26	1.43±0.20	0.75±0.04	0.54±0.05	1.88±0.18

Table 2

Oval window size and shape descriptive statistics according to age groupings with respect to sex.

Age Grouping	Sex	n	Size Parameters (Mean±SD)			Shape Parameters (Mean±SD)		
			Area (mm^2)	Width (mm)	Height (mm)	Circularity	Roundness	Aspect Ratio
Child	F	5	2.80±0.72	2.52±0.15	1.39±0.28	0.74±0.06	0.53±0.09	1.90±0.28
	M	9	2.87±0.64	2.66±0.20	1.39±0.17	0.74±0.03	0.52±0.04	1.93±0.14
	F+M	14	2.85±0.65	2.61±0.19	1.39±0.21	0.74±0.04	0.53±0.06	1.92±0.19
Adult	F	9	3.28±0.49	2.69±0.21	1.57±0.19	0.77±0.03	0.56±0.04	1.82±0.14
	M	8	2.79±0.55	2.55±0.25	1.41±0.17	0.74±0.02	0.53±0.04	1.89±0.14
	F+M	17	3.05±0.57	2.63±0.23	1.50±0.19	0.75±0.03	0.54±0.04	1.85±0.14
Child + Adult	F	14	3.11±0.61	2.63±0.20	1.51±0.23	0.76±0.04	0.55±0.06	1.85±0.20
	M	17	2.83±0.58	2.61±0.23	1.40±0.17	0.74±0.03	0.53±0.04	1.91±0.14
	F+M	31	2.96±0.60	2.62±0.21	1.45±0.20	0.75±0.04	0.54±0.05	1.88±0.17

Table 3

Results of canonical variates analysis including Mahalanobis distances among groups and *p*-values from permutation tests (10,000 permutation rounds) for Mahalanobis distances among groups.

	Fetus/Infant	Child	Adult
Fetus/Infant	–	3.1773	2.6113
	–	$p=0.0002$	$p=0.0380$
Child	3.1773	–	3.2060
	$p=0.0002$	–	$p<0.0001$
Adult	2.6113	3.2060	–
	$p=0.0380$	$p<0.0001$	–